Derepression of transposable elements enhances interferon beta signaling and stem/progenitor cell activity after proton irradiation

Davide Cinat[1,2*], Ryan van der Wal[1,2], Mirjam Baanstra[1,2], Abel Soto-Gamez[1,2], Anne L. Jellema-de Bruin[1,2], Marc-Jan van Goethem[2], Marcel A.T.M. van Vugt[3], Lara Barazzuol[1,2*], Rob P. Coppes[1,2*]

Affiliations

[1]Department of Biomedical Sciences, Section of Molecular Cell Biology, University Medical Center Groningen, University of Groningen, Groningen, The Netherlands.

[2]Department of Radiation Oncology, University Medical Center Groningen, University of Groningen, Groningen, The Netherlands.

[3]Department of Medical Oncology, University Medical Center Groningen, University of Groningen, Groningen, The Netherlands.

*Corresponding authors: d.cinat@umcg.nl (D.C.), l.barazzuol@umcg.nl (L.B), r.p.coppes@umcg.nl (R.P.C)

Summary

The release and subsequent detection of nucleic acids into the cytoplasm constitute a hallmark of the radiation-induced DNA damage response. However, different radiation types, such as photons and protons, may elicit distinct DNA damage responses, uniquely influencing normal stem cell activity and tissue regeneration. Here, we show that proton irradiation leads to enhanced derepression of transposable elements (TEs) with consequent activation of salivary gland stem/progenitor cells. This response is mediated by a pronounced loss of heterochromatin regulators and accumulation of cytoplasmic TE-derived dsRNA, resulting in upregulation of RIG-I and augmented interferon-beta (IFN-β) signaling. Single cell RNA sequencing (scRNA-seq) and TE dynamics analyses corroborate these findings, specifically in a subpopulation of *Sox9*-expressing stem/progenitor cells with increased INF-β response. These data reveal that the presence of TE-derived IFN-β in the microenvironment of irradiated organoids increases stem/progenitor cell activity and organoid growth, pointing to advantages of proton therapy over photon-based radiotherapy.

Introduction

The DNA damage-induced immune response is an intricate process culminating in the induction of the inflammatory and immune response[1,2]. However, DNA damage-induced inflammation has predominantly been studied in tumor models[3–5], overlooking its potential significance in non-transformed tissues that also undergo DNA damage during cancer treatment. Adult normal tissue stem cells are crucial for regenerating damaged tissues[6], and their proliferation and self-renewal capacity are influenced by stress-induced microenvironmental changes, including DNA insults[1,7,8]. Indeed, the expression of type 1 interferons (IFN1) can be triggered by radiation-induced DNA damage[7,9], leading to the activation of an immune response. However, the exact mechanisms underlying the induction of IFN1 expression and the subsequent impact of IFN1 signaling on normal tissue stem cells remain largely unclear. Moreover, the normal tissue response may vary depending on the complexity of DNA damage induced by different radiation modalities, as evidenced in the context of proton therapy compared to conventional photon-based radiotherapy for cancer treatment[10]. Indeed, recent studies have revealed that proton irradiation can elicit distinct DNA damage responses and activate specific pathways[11–13], leading to more effective killing of cancer cells[11,14]. However, to date, the understanding of the molecular effects of proton versus photon irradiation on normal tissue is still limited. In this regard, we used mouse salivary gland organoids enriched in stem and progenitor cells[15] as a model to investigate the response of normal tissue to photon and proton irradiation. We show that proton irradiation elicits a higher IFN-β response via derepression of TEs and cytoplasmic dsRNA formation, ultimately enhancing stem/progenitor cell activity and self-renewal capacity.

Results

Proton irradiation leads to a higher INF-β response

Proton and photon irradiations led to a similar, dose-dependent decrease in the number of mature organoids and living cells at 6 days after irradiation (Figures S1A and S1B), as expected based on the similar relative biological effectiveness (RBE) of these two radiation types[16]. However, the organoids irradiated with 7 Gy protons

exhibited a higher self-renewal capacity than 7 Gy photons (Figures 1A-1C), suggesting a differential response in the stem/progenitor compartment of these organoids. To understand the mechanisms underlying this difference, bulk RNA-sequencing (RNA-seq) of organoids at 2 and 6 days after irradiation was performed (Figure 1D), which revealed profound radiation-induced transcriptional changes, involving strong upregulation of genes associated with immunity and inflammation (Figures S1C and S1D). In agreement with the observation that the IFN-β response appeared as one of the most enriched biological processes after irradiation (Figures 1E and S1E), several IFN-stimulated genes (ISGs) showed a higher expression at 6 days after proton compared to photon irradiation (Figures 1F, 1G and S2A-S2D). In line with these findings, higher protein levels of STAT1 and p-STAT1 were measured after proton irradiation, indicating a more pronounced activation of IFN-β/STAT1/ISGs signaling upon proton versus photon irradiation (Figures 1H, 1I and S2E).

cGAS and ZBP1 modulate interferon signaling after irradiation

Activation of the cGAS-STING pathway in response to cytoplasmic dsDNA is an established mechanism responsible for IFN-β activation upon DNA damage[17]. In line with this notion, normal tissue-derived organoids showed increased levels of micronuclei and cytoplasmic cGAS at 2 days after 7 Gy photon and proton irradiation, which were decreased at 6 days after irradiation (Figures 2A, 2B and S3A, S3B). Despite the lower amount of micronuclei and cytoplasmic cGAS levels at 6 days after irradiation, levels of cytoplasmic dsDNA remained high (Figure 2D). In line with a role for cGAS in driving ISG expression, treatment with the covalent STING inhibitor C-176 decreased ISG expression at 6 days after irradiation (Figure 2E), suggesting the involvement of dsDNA-induced STING signaling in the regulation of ISGs also at this time point. Nevertheless, the activation of the cGAS-STING pathway could not explain the difference in IFN-β response between photons and protons.

Since mitochondrial damage is associated with inflammation and IFN-β activation[18,19], we investigated whether mitochondrial dysfunction and the leakage of mitochondrial DNA (mtDNA) could explain the presence of high cytoplasmic dsDNA and IFN-β activation at 6 days after proton irradiation. Measurement of mitochondrial membrane potential and total mitochondrial mass showed an accumulation of dysfunctional mitochondria in photon- and proton-irradiated samples (Figure 3A).

Accordingly, irradiation resulted in significantly higher levels of cytosolic mtDNA in irradiated organoids (Figure 3B), which could be responsible for inflammatory signaling and immune responses[20,21]. To establish whether mtDNA contributes to the observed inflammatory response, we depleted mtDNA by treatment with non-cytotoxic concentrations of ethidium bromide (EtBr)[22] (Figures S4A-S4D). mtDNA depletion led to a pronounced decrease in ISG expression in irradiated samples (Figures 3C and S4E), confirming the involvement of mtDNA in the induction of IFN-β. Of note, mtDNA depletion led to a similar decrease in IFN-β induction upon photon and proton irradiation.

The low levels of cGAS detected at 6 days (Figure 2C) prompted us to explore whether the high expression of IFN-β at this time point was associated with the upregulation of other dsDNA sensors. ZBP1 (also known as DLM-1 or DAI) is a cytosolic nucleic acid sensor able to modulate the immune response upon recognition of different forms of dsDNA, including mtDNA[19,23]. RNA-seq analysis revealed *Zbp1* as one of the most upregulated genes at 6 days after irradiation (Figures 3D, S1C and S5A). Moreover, a significant increase in cytosolic ZBP1 levels was observed in irradiated organoids (Figures 3E and S5B). Importantly, ZBP1 expression decreased in EtBr-treated samples (Figures 3F and S5C), confirming a link between mtDNA and *Zbp1* upregulation. Depletion of cGAS pronouncedly reduced ISG expression and STAT1 levels (Figures 3G, 3H and S5D), confirming the upstream role of cGAS in the regulation of IFN-β/STAT1 signaling[24]. Notably, ZBP1 depletion also reduced the expression of ISGs (Figures 3I and S5E). Together, these data indicate that cGAS plays an essential role in the regulation of IFN-β signaling after radiation-induced DNA damage in normal tissue cells, while ZBP1 may further reinforce the inflammatory response by sensing mtDNA. However, activation of these pathways does not explain the differential IFN-β response observed after proton irradiation.

Proton-induced loss of histone H3 methylation leads to dysregulation of transposable elements

Gene set enrichment analysis (GSEA) revealed a significant upregulation of double-stranded (ds)RNA binding components at 6 days after irradiation (Figures 4A and S6A). Consistent with our previous data, several genes associated with this gene ontology term exhibited a higher expression upon proton compared to photon

irradiation (Figure S6B). Among these genes, the Rig-I like Receptors (RLRs) *Mda5* (or *Ifih1*) and *Rig-I* (or *Ddx58*), key modulators of the inflammatory response induced by detection of cytoplasmic dsRNA[25,26], were found to be highly upregulated especially with protons (Figure S6C). qPCR and western blot analysis confirmed a significantly higher increase of RIG-I at 6 days after 7 Gy proton irradiation (Figures 4B, 4C and S6D). Accordingly, microscopy analysis of organoid sections revealed a higher accumulation of dsRNA in the cytoplasm of 7 Gy proton-irradiated samples (Figure 4D, 4E and S6E, S6F), suggesting a link between increased cytoplasmic dsRNA levels and a subsequent activation of RIG-I, possibly explaining the higher IFN-β response upon proton irradiation.

Derepression of TEs has been shown to cause endogenous dsRNA accumulation[27–29]. Indeed, analysis of TE expression by bulk RNA-seq and qPCR showed a higher upregulation of several TEs at 6 days after proton irradiation, including endogenous retroviruses (such as ERVK and ERVL) and LINE-1 (L1) elements (Figures 4F, 4G). In accordance with this, we detected a stronger downregulation of histone variants *H3f3a* and *H3f3b*, several methyltransferase-related genes (Figure S7A) and global histone H3K9 methylation (H3K9Me) upon 7 Gy proton irradiation (Figures 4H, 4I and S7C), which are important regulators of the expression of coding genes as well as TEs[28–31]. Since H3K9Me is essential for the regulation of long terminal repeats (LTRs) and L1 elements[32], we next treated non-irradiated organoids with the H3K9Me transferase inhibitor BRD4770 (Figure S7D). BRD4770 treatment led to upregulation of ERVK, ERVL and L1 elements (Figure 4J), increased ISG expression and elevated STAT1 protein levels (Figures 4K-4M), highlighting a role for histone H3 methylation in regulating the activation of TEs and the downstream dsRNA-mediated IFN-β signaling pathway. Taken together, these data indicate that the difference in response to protons is related to the loss of histone H3K9Me, which leads to higher TE-related dsRNA formation.

INF-β enhances *Sox9*-expressing stem/progenitor cell activity after irradiation

Radiation-induced loss of genomic integrity and subsequent changes in its microenvironment can profoundly affect the self-renewal capacity and longevity of stem cells[7,33,34]. Given the stronger IFN-β response and self-renewal capacity observed upon proton irradiation, we explored whether IFN-β signaling in the irradiated

stem/progenitor cell microenvironment affects self-renewal potential. For this purpose, recombinant IFN-β was added to the culture media after photon irradiation and stem cell self-renewal capacity was assessed (Figure S7E). Interestingly, while no changes were observed in control samples, photon-irradiated organoids exhibited enhanced cell proliferation in response to IFN-β treatment (Figure 5A and S7F).

To analyze the effects of photon and proton irradiation on the different cell populations within the organoids, we performed scRNA-seq. Analysis of the integrated dataset using established markers[35,36] (Figures 5B, 5C and S8A) revealed the presence of a population of ductal cells expressing *Krt7, Krt8,* and *Krt19*; a population of stem/progenitor cells expressing *Sox9* and *Wnt4*; two populations of differentiating cells expressing *Aqp5, Acta2,* and *Krt19*; a population of progenitor cells expressing *Cd44, Chrm3,* and *Lgr4;* populations of proliferating cells expressing *Mki67* and *Top2a;* and, senescent cells expressing *Cdkn2a* and *Cdkn1a*. Notably, although these cell populations were identified among the different conditions (Figure S8B), analysis of the non-integrated dataset revealed strong differences in the distribution of these cell populations after irradiation between photons and protons (Figure 5D). In fact, in line with the previous results, proton-irradiated cells exhibited a higher expression of several ISGs, such as *Ifi27l2a*, *Ifi44,* and *Ifih1,* compared to the other conditions (Figure S8C).

The identified population of *Sox9+* cells (Figures 5C, 5E left panel and S8D) reflects a stem/progenitor cell population involved in tissue development and regeneration following irradiation in several tissues[37–39]. Although cells from all irradiated clusters showed increased expression of IFN-related genes (Figures 5E right panel and S8E), proton-irradiated *Sox9+* cells exhibited a stronger upregulation of IFN-β (Figures 5E, 5F and S8D). Furthermore, microscopy analysis of organoid sections (Figures 5G and S8F) revealed higher protein levels of STAT1 in SOX9+ cells following proton irradiation (Figure 5H), suggesting a more prominent response of this stem/progenitor cell population to IFN-β. Further cluster analysis of the scRNAseq data of control samples revealed a sub-population of *Sox9+* cells enriched with proliferation markers, such as *Mki67* and *Top2a* (Figures 5I and S5G). Interestingly, differential gene expression and gene set enrichment analysis (GSEA) within this cluster of cells after photon and proton irradiation, showed a stronger downregulation of processes related to cell proliferation and cell cycle progression upon photon compared to proton irradiation (Figure 5J), which agrees with the lower self-renewal capacity of photon-

irradiated organoids (Figure 1C). Together, these findings suggest that the higher IFN-β response triggered by proton irradiation may enhance the activity and proliferation of *Sox9+* stem/progenitor cells resulting in an increased organoid formation efficiency (OFE) and self-renewal ability.

Since the higher IFN-β response detected upon proton irradiation was associated with an increased expression of several TEs (Figure 4F, 4G), we explored individual TEs at the single cell level. We identified a stronger upregulation of several TEs in the clusters of proton-irradiated cells (Figures S9A and S9B), including the *B2_Mm2* TE, which was shown to be a potent IFN-β enhancer[40]. Interestingly, cells expressing a high TE score and ISGs exhibited lower expression of the *H3f3a* and *H3f3b* genes (Figures 5K and S9C), which are key heterochromatin regulators involved in TE silencing[30]. These results reiterate the link between TE upregulation and heterochromatin decondensation in relation to proton irradiation-induced IFN-β responses in stem/progenitor cells.

Discussion

We demonstrate that proton irradiation induces a more pronounced upregulation of TEs and enhanced RIG-I-mediated IFN-β signaling compared to conventional photon irradiation. Our findings reveal a link between proton-induced heterochromatin decondensation, TE deregulation and cytoplasmic dsRNA formation, resulting in the upregulation of ISGs and ultimately leading to enhanced stem/progenitor cell activity and self-renewal capacity.

Activation of the cGAS-STING pathway following micronuclei formation is known to be a major driver of IFN-β induction upon radiation-induced DNA damage in cancer cells and transformed cell lines[17]. Using a salivary gland organoid model, reflective of normal tissue stem cells[15,41–43], we show a significant increase of cytoplasmic cGAS and micronuclei formation at 2 days after photon and proton irradiation. Notably, these levels decrease at 6 days, which can be attributed to the propensity of micronucleated cells to undergo cell death or apoptosis[44]. Moreover, although the fate of micronuclei remains largely unclear, studies suggest that they may undergo degradation or reincorporation into the nucleus over time[44,45], offering an alternative explanation for their reduced number at later time points.

Similar to nuclear DNA, the release of mtDNA due to mitochondrial dysregulation can also activate cytoplasmic nucleic acid sensors, leading to inflammation[18]. Our study reveals that photon and proton irradiation induce a simultaneous accumulation of damaged mitochondria and cytoplasmic dsDNA and mtDNA at 6 days post-irradiation. This aligns with previous work of us [46] and others[47], showing a correlation between the accumulation of elongated-damaged mitochondria and the upregulation of IFN-β following mtDNA leakage into the cytoplasm. The low levels of cGAS, however, suggest the involvement of other cytoplasmic nucleic acid sensors, such as ZBP1[48]. In fact, abrogation of ZBP1, along with the depletion of mtDNA, significantly decreases ISG expression upon irradiation, confirming its crucial role in the prolonged IFN-β response[19,23]; nevertheless, without explaining the difference in response to protons and photons.

Although the IFN-β response observed after irradiation is largely mediated by the activation of cytoplasmic dsDNA sensors, proton-irradiated organoids display a higher increase of TE expression, accompanied by an accumulation of cytoplasmic dsRNA and upregulation of the dsRNA sensor RIG-I. Elevated levels of TEs, dsRNA, and RIG-I have been shown to enhance the immune response of cancer cells following irradiation[49]. However, our study reveals that this phenomenon extends beyond tumors, as irradiated non-tumor cells also express these immune-enhancing elements. This emphasize the pivotal role of TEs in enhancing IFN1 response not only in tumors and age-associated disorders[29,50–52] but also in irradiated normal tissue-derived stem/progenitor cells. Importantly, TEs are tightly regulated, and their expression can be profoundly affected by alterations in chromatin accessibility[28,31]. We demonstrate that proton irradiation leads to a more pronounced loss of histone H3K9Me and downregulation of the histone variants *H3f3a* and *H3f3b* at 6 days, pivotal factors in TE silencing[53]. Consistent with our findings, previous studies have shown a differential epigenetic modulation and downregulation of histone H3 methylation in various tumors following proton irradiation[12].

Although protons elicit a stronger IFN-β response, proton-irradiated organoids show enhanced self-renewal capacity compared to photon-irradiated organoids, reflecting higher stem cell activity and proliferation. We show that treatment of photon-irradiated organoids with IFN-β enhances OFE, which aligns with the heightened self-renewal capacity observed in proton-irradiated cells. Recent studies have demonstrated that the presence of cGAS-STING-dependent-IFN-β in the niche of

irradiated-intestinal stem/progenitor cells[9], as well as the activation of TEs in chemotherapy-treated hematopoietic stem cells[55], improved tissue regeneration. Our scRNAseq analysis further support these findings, revealing a cluster of cells with highly upregulated TEs and a robust IFN-β response, which leads to increased proliferation of *Sox9+* stem/progenitor cells following proton irradiation.

With our study establishing a clear correlation between the higher self-renewal capacity of proton-irradiated organoids and the increased upregulation of TEs and related IFN-β response *in vitro*, further studies are warranted to validate the potential clinical implications *in vivo* and to evaluate the combined effects of IFN-β activation and the immune response. Furthermore, while proton irradiation is used to deliver a higher dose to the tumor, potentially enhancing cancer cell killing, it is also important to assess the effects of alterations in the tumor microenvironment on cancer stem cell proliferation and plasticity. Optimizing the balance between cancer cell elimination and the enhancement of normal stem cell function and tissue regeneration is essential, as it can significantly contribute to improving patient outcomes post-cancer treatment.

Acknowledgments

This work was supported by the Dutch Cancer Society KWF Grant nr 12092. We would like to thank S. Both, J. Free and B.N. Jones for the technical support at the PARTREC and GPTC; B. Eggen and his group for support and advise in the scRNA-seq library preparation and analysis; the members of the ERIBA Research Sequencing Facility (UMCG) for the sequencing runs; the members of Flow Cytometry Unit (UMCG) for the sorting and the members of the UMCG Microscopy & Imaging Center for the microscopy and imaging support. Illustrations were created with BioRender.com.

Author contributions

D.C, L.B and R.P.C conceived and designed the study. D.C., R.v.d.W, M.B., A.S.G and A.L.J.D.B. performed the experiments and analyzed the data. D.C. and M.J.v.G. performed the irradiations. D.C., L.B. and R.P.C. wrote the manuscript with advice and input from M.A.T.M.v.V. All the authors approved the manuscript.

Declaration of interests

The authors declare no competing interests.

Figures

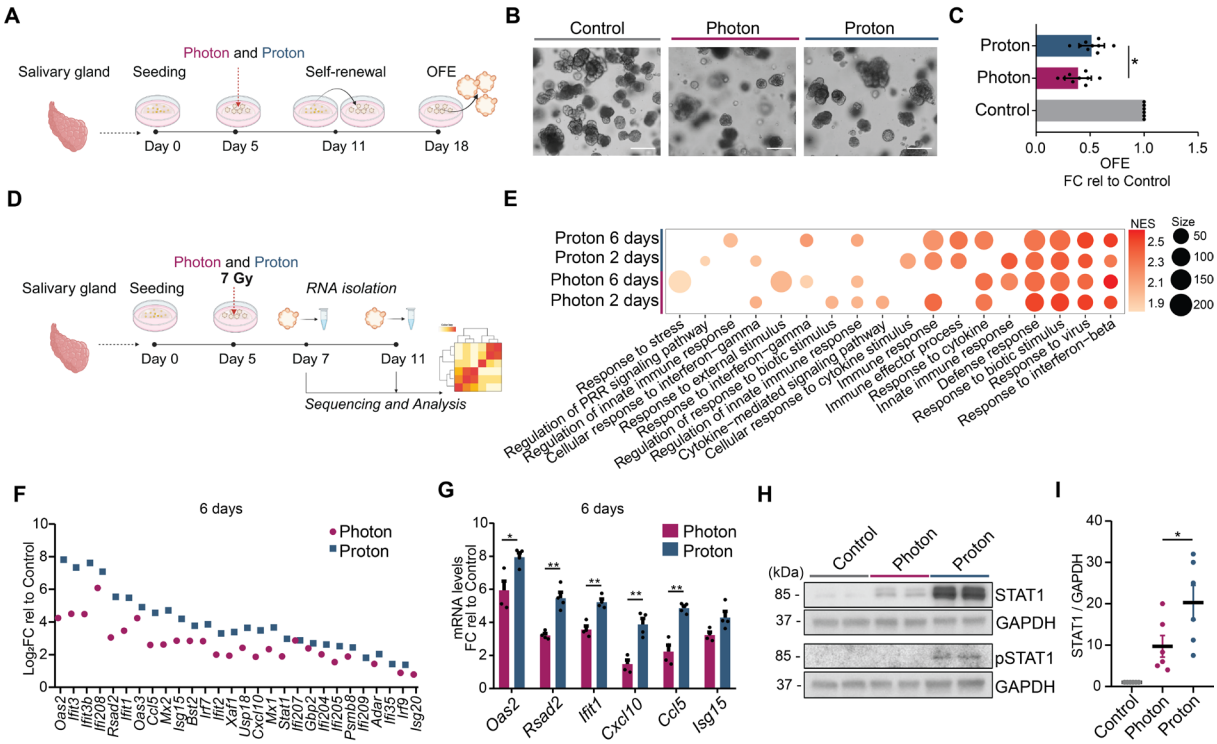

Figure 1: Proton-irradiated organoids show a higher self-renewal capacity and IFN-β response compared to photons.

(A) Schematic representation of the self-renewal assay. Organoids were irradiated at day 5 and quantification shown as percentage of organoid forming efficiency (OFE%) was calculated after self-renewal at day 18.

(B) Representative images of organoids in culture after self-renewal. Scale bar, 100 µm.

(C) Organoid quantification shown as OFE fold change (FC) relative to control samples. n = 9 animals/condition.

(D) Schematic representation of the bulk RNA-seq analysis. RNA was isolated from organoids at 2 days (day 7) and 6 days (day 11) post irradiation.

(E) Top 10 significant (p.adj. < 0.05) biological processes in proton vs control and photon vs control at 2 and 6 days post irradiation.

(F) Gene expression level of significant ($p < 0.05$) ISGs extrapolated from the bulk RNA-seq data of organoids at 6 days post irradiation. Data is shown as Log_2FC relative to control samples.

(G) rt-qPCR analysis of ISGs at 6 days post irradiation. Data is shown as FC relative to control samples. n = 4 animals/condition.

(H) Western blot analysis of STAT1, pSTAT1 and GAPDH of organoids at 6 days post irradiation.

(I) Western blot quantification of STAT1 (Figures 1I and S2E). STAT1 protein levels were normalized for GAPDH. Data is shown as FC relative to control samples. n = 6 animals/condition.

Data are means ± s.e.m. Student's t-test and two-way ANOVA. *$p < 0.05$, **$p < 0.01$.

See also Figures S1 and S2.

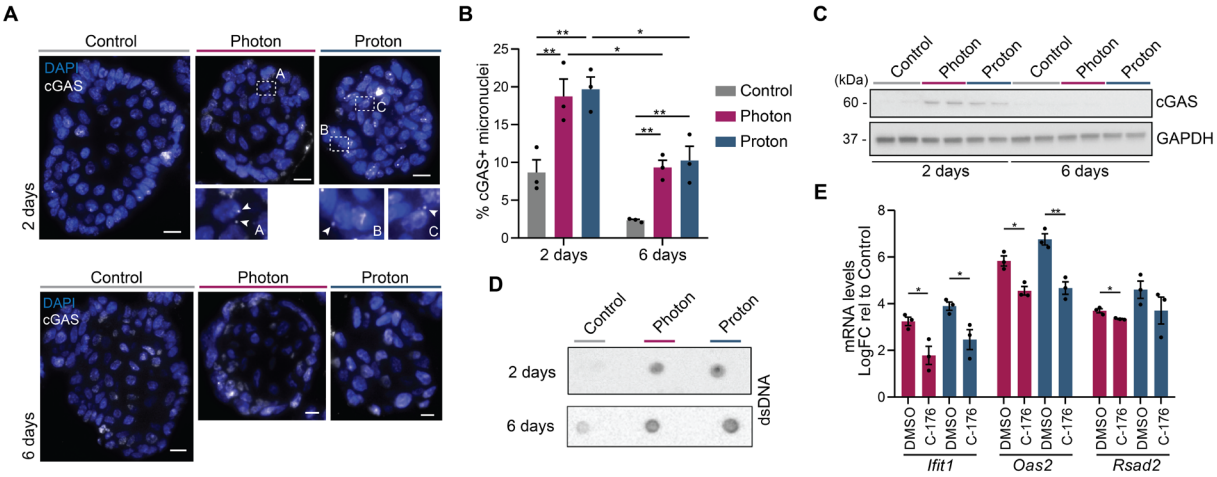

Figure 2: Radiation induces micronuclei formation and cytoplasmic cGAS upregulation.

(A) Representative images of immunofluorescence staining of organoids sections at 2 days (top) and 6 days (bottom) post irradiation. Zoom-ins and arrows show cGAS+ micronuclei. Scale bar, 5 µm.

(B) Quantification of cGAS+ micronuclei at 2 and 6 days. Data is shown as percentage (%) of cGAS+ micronucleated cells/total number of cells. n = 3 animals/condition.

(C) Western blot analysis of cGAS and GAPDH of cytoplasmic fractions extracted from organoids at 2 days and 6 days post irradiation. Validation of the fractionation is shown in Figure S3B.

(D) Dot blot analysis of dsDNA of cytoplasmic fractions extracted from organoids at 2 days and 6 days post irradiation.

(E) rt-qPCR analysis of ISGs in DMSO and C-176-treated organoids at 6 days post irradiation. Data is shown as FC relative to DMSO control. n = 3 animals/condition.

Data are means ± s.e.m. Student's t-test. *p < 0.05, **p < 0.01.

See also Figure S3.

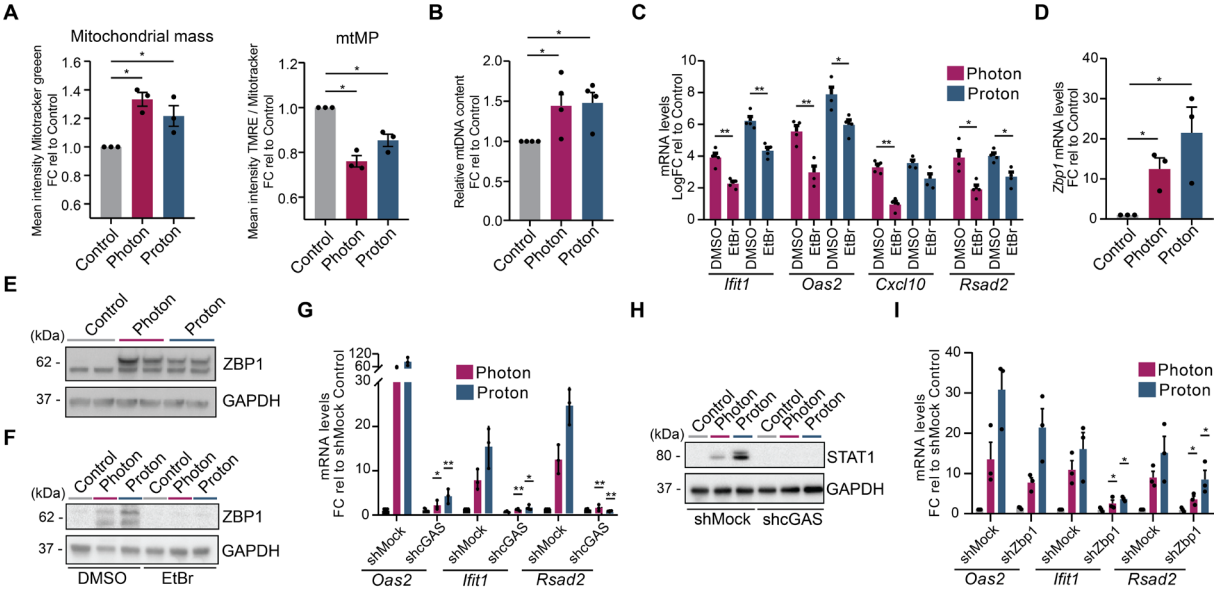

Figure 3: Radiation-induced mitochondrial dysfunction leads to mtDNA leakage and ZBP1 upregulation.

(A) Flow cytometry analysis showing the mitochondrial mass (left panel) and mitochondrial membrane potential (mtMP) (right panel) at 6 days post irradiation. Data is shown as FC relative to control. n = 3 animals/condition.

(B) rt-qPCR analysis of mtDNA genes of cytoplasmic fractions of organoids at 6 days post irradiation. Data is shown as mean expression of *mt16S, mtCOX2, mtDloop3*. Data is shown as FC relative to control samples. n = 3 animals/condition.

(C) rt-qPCR analysis of ISGs in DMSO and EtBr-treated organoids at 6 days post irradiation. n = 4 animals/condition.

(D) rt-qPCR analysis of *Zbp1* at 6 days post irradiation. n = 3 animals/condition.

(E) Western blot analysis of ZBP1 and GAPDH of cytoplasmic fractions extracted from organoids at 6 days post irradiation.

(F) Western blot analysis of ZBP1 and GAPDH in DMSO and EtBr-treated organoids at 6 days post irradiation.

(G) rt-qPCR analysis of ISGs in shMock and shcGAS-treated organoids at 6 days post irradiation. Data is shown as FC relative to shMock control. *p and **p are relative to shMock. n = 3 animals/condition.

(H) Western blot analysis of STAT1 and GAPDH in shMock and shcGAS-treated organoids at 6 days post irradiation.

(I) rt-qPCR analysis of ISGs in shMock and shZBP1-treated organoids at 6 days post irradiation. Data is shown as FC relative to shMock control. *p is relative to shMock. n = 3 animals/condition.

Data are means ± s.e.m. Student's t-test. *p < 0.05, **p < 0.01.

See also Figure S4 and S5

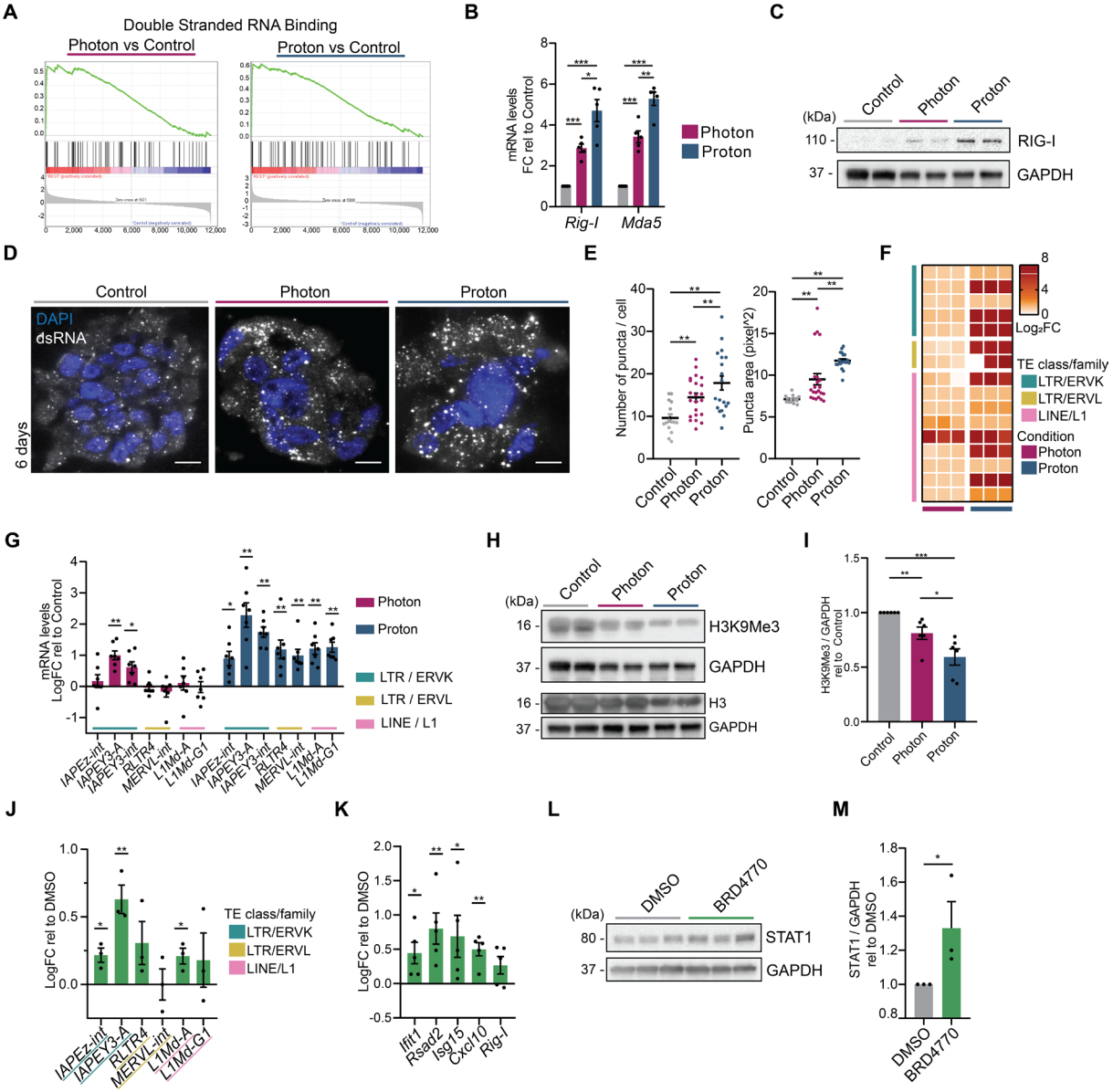

Figure 4: Proton irradiation leads to a higher upregulation of TEs and accumulation of dsRNA into the cytoplasm.

(A) Enrichment plots of the biological process double stranded RNA binding at 6 days post photon and proton irradiation.

(B) rt-qPCR analysis of *Rig-I* and *Mda5* at 6 days post irradiation. Data is shown as FC relative to control. n = 6 animals/condition.

(C) Western blot analysis of RIG-I and GAPDH of organoids at 6 days post irradiation.

(D) Representative images of immunofluorescence staining of organoids sections at 6 days post irradiation. Scale bar, 10 µm.

(E) Immunofluorescence staining quantification showing the number of dsRNA puncta (left panel) and puncta mean area (right panel).

(F) Gene expression level of significant ($p < 0.05$) TEs extrapolated from the bulk RNA-seq data of organoids at 6 days post irradiation. Data is shown as Log_2FC relative to control samples.

(G) rt-qPCR analysis of TEs at 6 days post irradiation. Data is shown as a FC relative to control. n = 6 animals/condition.

(H) Western blot analysis of H3K9Me, H3 and GAPDH of organoids at 6 days post irradiation.
(I) Western blot quantification of H3K9Me3 (Figures 4H and S7B). H3K9Me3 protein levels were normalized for GAPDH. n = 6 animals/condition.
(J) rt-qPCR analysis of TEs in BRD4770 and DMSO-treated organoids at day 11. Data is shown as Log_2FC relative to DMSO.
(K) rt-qPCR analysis of ISGs in BRD4770 and DMSO-treated organoids at day 11. Data is shown as Log_2FC relative to DMSO.
(L) Western blot analysis of STAT1 and GAPDH in BRD4770 and DMSO treated-organoids at day 11.
(M) Western blot quantification of STAT1 (Figure 4L). STAT1 protein levels were normalized for GAPDH. n = 3 animals/condition.
Data are means ± s.e.m. Student's t-test and two-way ANOVA. *$p < 0.05$, **$p < 0.01$, ***$p < 0.005$.
See also Figures S6 and S7.

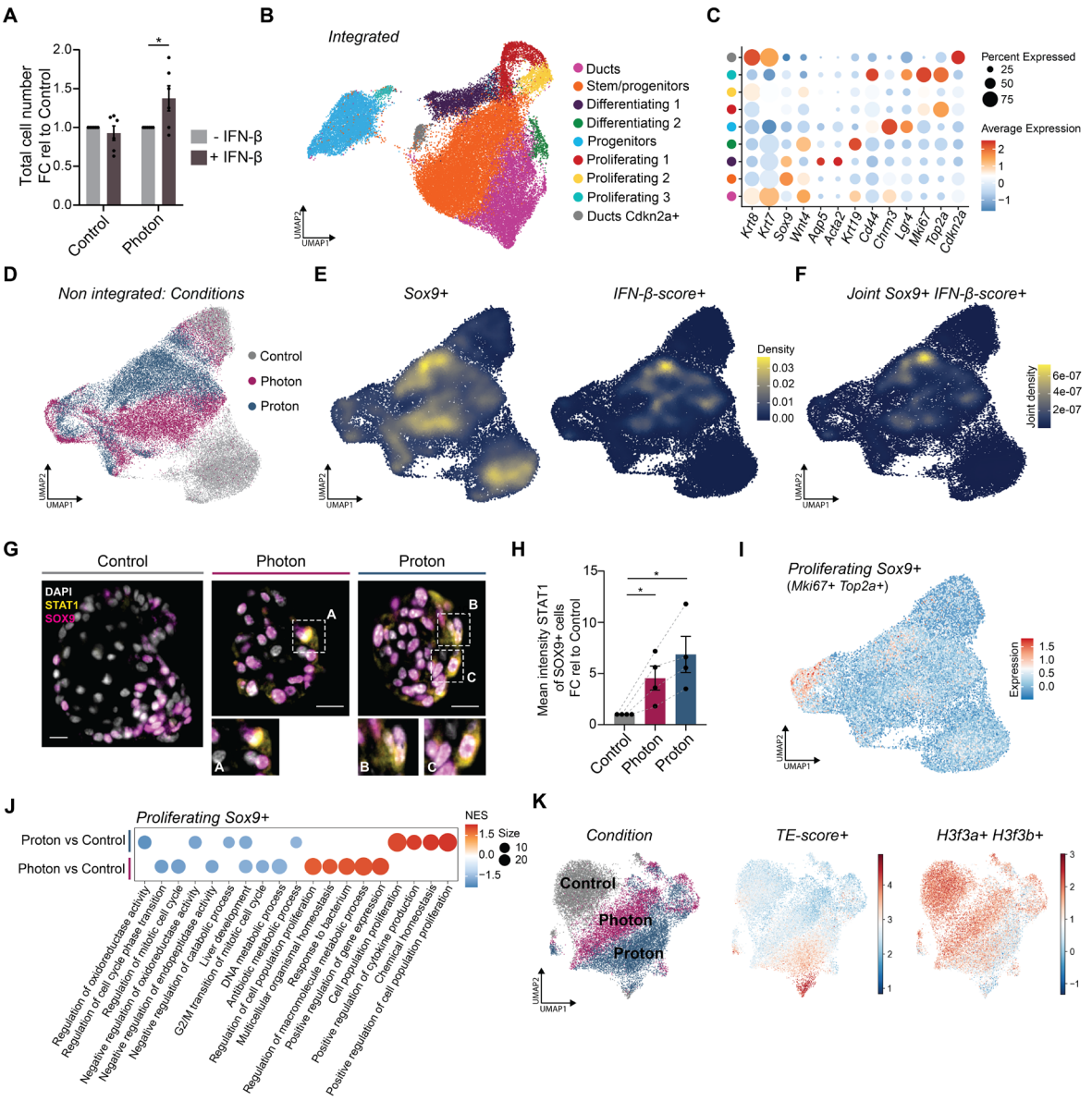

Figure 5: Salivary gland *Sox9+* stem/progenitor cells show a higher IFN-β response and activity after proton irradiation.

(A) Quantification of the total number of cells of control and photon-irradiated organoids after self-renewal (day 18) and treatment with (+) or without (-) IFN-β. Data is shown as FC relative to untreated organoids. n = 6 animals/condition.

(B) UMAP of the integrated dataset of organoids at 6 days post irradiation (day 11) showing the main cell populations.

(C) Dot plot showing representative cell type marker genes for each population, cluster colors are the same as in Figure 4B.

(D) UMAP of the non-integrated dataset of organoids at 6 days post irradiation (day 11) showing the different conditions.

(E) Density plot of the non-integrated dataset of organoids at 6 days post irradiation (day 11) showing *Sox9* expression (left panel) and IFN-β-score (*Ifih1*, *Ifi44*, *Stat1* and *Ifi27l2a*) (right panel).

(F) Density plot of the non-integrated dataset of organoids at 6 days post irradiation (day 11) showing the joint expression of *Sox9* and IFN-β-score (*Ifih1*, *Ifi44*, *Stat1* and *Ifi27l2a*).

(G) Representative images of immunofluorescence staining of organoids sections at 6 days post irradiation. Scale bar, 10 µm.
(H) Quantification of STAT1 mean intensity in SOX9+ nuclei. Dotted lines link the same animal across different conditions. n = 4 animals/condition.
(I) UMAP of the non-integrated dataset of organoids at 6 days post irradiation (day 11) showing the co-expression of *Sox9, Mki67* and *Top2a*.
(J) Top 10 significant (p.adj. < 0.05) up- and downregulated biological processes in proton vs control and photon vs control in the proliferating *Sox9+* cells. Dot color represents normalized enrichment score (NES), dot size (Size) represents gene number.
(K) UMAPs of the non-integrated dataset of organoids at 6 days post irradiation (day 11) re-analyzed considering both genes and TEs showing: the different conditions (left panel); cells expressing *MTE2b, B2_Mm2, RSINE1, M1_Mus2, B1_Mus1* and *B3* (TE-score) (central panel); cells expressing *H3f3a* and *H3f3b* (right panel).
Data are means ± s.e.m. student's t-test. *p < 0.05.
See also Figures S7, S8 and S9.

Methods

The details of all antibodies and reagents used in this study are listed in Table S1.

Mice

For the culturing of salivary gland organoids, 8-to 12-week-old female C57BL/6 mice (Envigo, the Netherlands) were used. Mice were housed under conventional conditions with a standard diet and water *ad libitum* at the central animal facility of the University Medical Center Groningen. Animal experimental procedures were approved by the Central Committee of Animal Experimentation of the Dutch government and the Institute Animal Welfare Body of the University Medical Center Groningen [animal welfare body (IVD) protocol number 184824-01-001].

Organoid culture and self-renewal assay

Following the collection of submandibular salivary glands, tissue isolation was performed as previously described[56]. In summary, after mechanic and enzymatic digestion, cells were cultured in DMEM/F12 complemented with penicillin-streptomycin (Pen/Strep) antibiotics, glutamax (2 mM), EGF (20 ng/ml); FGF2 (20 ng/ml), N2 (1x), insulin (10 µg/ml) and dexamethasone (1 uM). After 72 hours in culture, primary spheres were dissociated into single cells using 0.05% trypsin EDTA and counted. 10.000 cells were then plated in 75 µL gel/well [35 µL cell suspension + 40 µL of culturex basement membrane extract Type 2 (BME)] or [25 uL cell suspension + 50 uL of Matrigel] in a 12-well tissue culture plate. After solidification of the gels, 1 mL of WRY medium [DMEM/F12, penicillin-streptomycin, glutamax, N2, EGF, FGF2, insulin, Y27632 (10 µM), 10% R-spondin1–conditioned medium, and 50% Wnt3a-conditioned medium] was added to each well. The gels were then incubated at 37°C and 5% CO_2 until the day of the experiment.

Organoid irradiation and treatments

Irradiation

After 5 days in culture, mouse salivary gland organoids were irradiated either with 4, 7 and 15 Gy photons using a Cesium-137 source (dose rate of 0.59 Gy/min) at the department of Biomedical Sciences of the UMCG or with 4, 7 and 15 Gy plateau protons (150 MeV, dose rate of 4 Gy/min) at the Particle Therapy Research Center (PARTREC) accelerator facility of the UMCG and at the UMCG Proton Therapy Center (GPTC).

Drug treatments

C-176 (0.5 μM) or equivalent volume of solvent (DMSO) was added to the media of irradiated and non-irradiated organoids at 1 day and 4 days after irradiation; BRD4770 (1.5 μM) or equivalent volume of solvent (DMSO) was added to the media of 7 day-old non-irradiated organoids; IFN-β was added to the media of photon-irradiated and non-irradiated organoids at day 7 at a final concentration of 2 ng/mL and at the time of self-renewal at a final concentration of 0.5 ng/mL; and, for an effective depletion of mtDNA, organoids were treated with Ethidium Bromide (EtBr) from day 2 at a final concentration of 100 ng/mL.

Bulk RNA-sequencing library preparation

For the cDNA library preparation, total RNA was extracted from organoids at 2 (day 7) and 6 days (day 11) post irradiation using RNeasy Mini Kit according to the manufacturer's instructions. RNAquality was determined using High Sensitivity RNA ScreenTapes on an Agilent 2100 Bioanalyzer. Highly intact RNA (RIN value > 9) from organoids derived from 3 different animals/condition was then processed for the cDNA library preparation using the QuantSeq 3' mRNA-Seq Library Prep Kit following the manufacturer's protocol; 100 ng of RNA was used as an input for all samples. Libraries were equimolarly pooled and 1.8 pM of the pool with 15% PhiX were loaded on a NextSeq 500 (Illumina) for a 75 bp single-read sequencing run at the Research Sequencing Facility of ERIBA (UMCG).

Bulk RNA-sequencing analysis

For the alignment of the fastq files the mouse genome GRCm39 was used. The gene counts per sample were detected with the QuantSeq 3' mRNA-seq Integrated Data Analysis Pipeline on the BlueBee Genomics Platform provided by Lexogen with default settings. R (v4.1.3) and RStudio were used for the downstream analysis and plots were generated with the R package ggplot2[57]. For the differential expression analysis, low expressed genes (total count <1 in less than 2 samples) were excluded. The R package edgeR[58] was used for normalization and identification of differential expressed genes (LogFC > 0.6, FDR < 0.05). Gene set enrichment analysis (GSEA) for differentially expressed genes and reduction of redundant gene ontology (GO) terms were performed with the R packages clusterProfiler[59] and Revigo[60]. GO terms with an adjusted *P* value < 0.05 were considered significant.

For the identification of TEs, the R package Rsubread[61] was used for the annotation upon alignment of the fastq files on the mouse genome GRCm39. The database gEVE version 1.1 was used to retrieve the annotation datasheet. The R package edgeR was then used for downstream analysis and identification of differentially expressed TEs (logFC > 0.6, FDR < 0.05).

Western blot

After harvesting, organoids were lysed using RIPA buffer, sonicated and spun down at 4°C (for 5 min at max speed). The protein concentration of the lysates was measured using the Bradford quantification method and the samples were boiled at 99°C for 5 min before loading. An equal amount of protein was separated with 10 or 12% polyacrylamide gels. The transfer to nitrocellulose membranes was performed using the Trans-Blot Turbo System (Bio-Rad). Blocking was performed using 10% milk in PBS-Tween20 for 30 min. After cutting, the membranes were incubated with primary antibodies at 4°C overnight followed by incubation with horseradish peroxidase-conjugated secondary antibodies at room temperature for 1.5 hours. Membranes were developed using ECL reagent in a ChemiDoc imager (Bio-Rad). Western blots analysis was performed using Image Lab software. The list of primary antibodies and dilutions are specified in Table S1.

Quantitative real-time qPCR

Total RNA was extracted from organoids by using RNeasy Mini Kit according to the manufacturer's instructions. cDNA reverse transcription was performed by using 1 µL dNTP mix (10 mM), 1 µL random primers (100 ng), 4 µL 5x First-strand Buffer, 2 µL DTT (0.1 M), 1 µL RNase OUTTM (40 units/µL), and 1 µL M-MLV RT (200 units). To assess the expression of the genes of interest, specific primers were used together with iQ SYBR Green Supermix. All reactions were run in triplicate on a Bio-Rad Real-Time PCR System. The list of primers is specified in Table S2. The *Ywhaz* gene was used as internal control.

Immunofluorescence staining

For the staining of micronuclei, 7 and 11 day-old salivary gland organoids were harvested and dissociated into single cells. After counting, cells were re-seeded at a concentration of 90.000 cells/well on the top of a coverslip in a 24 well plate. WRY media was added and cells were incubated at 37°C and 5% CO_2 overnight. On the next day cells were fixed with 4% formaldehyde and incubated with cGAS primary antibody followed by incubation with the proper secondary antibody, both at room temperature for 1 hour. DAPI was used for nuclear staining. Images were acquired with a Leica DM6 microscope.

For the staining of organoid sections, 7 and 11 day-old organoids were harvested and fixed with 4% formaldehyde. The organoids were then processed for embedding in paraffin and cut into 4 µm thick sections. For the staining of cGAS and dsRNA, sections were dewaxed and incubated with the proper primary antibody at 4°C overnight. On the next day, sections were incubated with the secondary antibody at room temperature for 1 hour. DAPI was used for nuclear staining. For the co-staining of SOX9 and STAT1 the Opal 4-Color anti-Rabbit Manual IHC Kit was used following the manufacturer' protocol. The Opal520 fluorophore was used to visualize STAT1 while the Opal570 fluorophore was used to visualize H3K9Me. Spectral DAPI was used for nuclear staining. Images were acquired with a Leica SP8X confocal microscope. The list of antibodies and dilutions are specified in Table S1. Images were analyzed using ImageJ (v1.52). Puncta analysis was performed using Icy (v2.4.2.0).

Subcellular fractionation

After harvesting, organoids were resuspended in subcellular fractionation buffer [Sucrose (250 mM), HEPES pH 7.4 (20 mM), KCl (10 mM), $MgCl_2$, EDTA (1 mM), EGTA (1 mM) and DTT (1 μM)], passed through a needle 10 times and placed on ice for 30 min. The lysates were then centrifuged at 720 xg for 5 min at 4°C. The supernatant containing the cytoplasm fraction was collected and spun at 10.000 xg for 5 min at 4°C. The supernatant was then concentrated through an Amicon Ultra-4 Filter Unit (Merck, cat#UFC8100214). The validation of the cytoplasm fraction was performed by western blot using antibodies against markers for nucleus (H2A), mitochondria (TOMM20) and cytoplasm (GAPDH). A whole cell extract from control samples was used as a positive control.

Dot blot

For the qualitative detection of dsDNA, the cytoplasm fractions from all the conditions were normalized based on their protein concentration (measured using the Bradford quantification assay). 2 μL of cytoplasm lysate was then placed on a nitrocellulose membrane and let dry at room temperature. After blocking with 10% milk in PBS-Tween20 at room temperature for 45 min, the membrane was incubated with dsDNA primary antibody for 1 hour followed by incubation with horseradish peroxidase-conjugated secondary antibody for 1 hour at room temperature. Membranes were developed using ECL reagent in a ChemiDoc imager. Dot blot analysis was performed using Image Lab software. The list of primary antibodies and dilutions are specified in Table S1.

Lentiviral production and transduction

For the lentiviral production HEK293T cells were plated with DMEM supplemented with 10% FBS, Pen/Strep and glutamax. Cells were then transfected with 3 μg of vector of interest (pLV[shRNA]-EGFP:T2A:Puro-U6>[shRNA]) (Vector Builder), 3 μg of packaging construct (PAX2), 0.7 μg of glycoprotein envelope plasmid (VSV-G) and 40 μL of PEI (1 μg/mL). On the next day, the media was replaced with DMEM/F12 and the viral supernatant was collected after 1 day.

For the transduction, salivary gland organoids were released from the gels and dissociated into single cells. After counting, the cell suspension was incubated with the

viral supernatant and polybrene (6 µg/mL) on a 24-well plate overnight at 37°C and 5% CO_2. On the next day, cells were counted and seeded in BME into a 12-well plate with WRY media. 2 days after seeding the media was supplemented with Puromycin (2 µg/mL) for the selection of the transduced cells and refreshed every 2 days. The efficiency of transduction was >95% for all the conditions and was assessed measuring the percentage of GFP positive cells.

Flow cytometry

To assess the total amount of mitochondria and their function following photon and proton irradiation, the dyes TMRE and Mitotracker Green were used. Briefly, salivary gland organoids were harvested, dissociated into single cells and resuspended with fresh culture medium supplemented with the probes at a final concentration of 200 nM. Cells were then incubated at 37°C and 5% CO_2 for 30 min and washed with PBS/BSA 0.2%. Cells were resuspended in PBS/BSA 0.2% and analyzed using the Quanteon flow cytometer at the Flow Cytometry Unit of the UMCG. Data was analyzed using the FlowJo software (v10.7.2).

Single cell RNA-sequencing library preparation

The preparation of the single cell RNA-sequencing library was performed by using the 10X Chromium Next GEM Single Cell 3' Kit v3.1, the 10X Chromium Next GEM Chip G Single Cell Kit and the 10X Single Index kit T Set A following the manufacturer's instructions. In brief, salivary gland organoids were collected and dissociated into single cells. On the same day, for the exclusion of death cells, 45.000 propidium iodide (PI) negative cells/samples were sorted using the Moflo Astrios sorter at the Flow Cytometry Unit at the UMCG. Organoids derived from 4 different mice/conditions were used and pooled at the time of the sequencing. After sorting, samples were loaded on the Chromium Next GEM Chip G and ran in the Chromium Controller (10X Genomics). On the next day, cDNA Amplification and library construction was performed following the manufacturer's protocol (10X Genomics). Libraries quality control and concentration measurements were performed using the Qubit and Tapestation machines at the Research Sequencing Facility of ERIBA at the UMCG. For the sequencing, libraries were equimolarly pooled and 1.8 pM of the pool with 5% PhiX

were loaded on a NextSeq 500 (Illumina) for a 75 bp paired-end sequencing run at the Research Sequencing Facility of ERIBA (UMCG).

Single cell RNA-sequencing analysis

Reads without cell barcodes or UMIs were excluded and remaining raw reads were aligned to the mouse genome GRCm39. Following demultiplexing and cell filtering, around 45.000 cells were used for downstream analysis (control 14.266 cells; photons 15.926 cells; protons 14.525 cells). Single cell RNA-sequencing analysis was done on R (v4.1.3) using the Seurat V4[62] package. Cells with more than 5% of mitochondria counts and less than 2500 feature counts were filtered out. Elbow plots and Jack Straw were used for the determination of the principal components (PC) to use for UMAP dimensionality reduction. Clusters with less than 100 cells and no relevant markers were excluded from the analysis and cluster-markers were identified using the FindAllMarkers function with the statistical test MAST.

Alignment and detection of TEs was performed on Python (v3.0) using the package scTE[63]. The downstream analysis was then performed using the Scanpy[64] package considering both genes and TEs. Clusters and marker genes/TEs were determined using the leiden algorithm and the wilcoxon statistical test.

Statistical analysis

Unpaired two-tailed Student's *t*-test and two-way ANOVA (mixed model) were used to determine significant differences between groups. Values are shown as mean ± s.e.m, as indicated in the figure legends. The number of biological replicates (n) used in each experiment is stated in the figure legend and p-values ≤ 0.05 were considered statistically significant. In each experiment the measurements were taken from different biological replicates, no samples were measured repeatedly. Statistical analyses were performed using the GraphPad Prism software (v8.0.1).

References

1. Cinat, D., Coppes, R.P., and Barazzuol, L. (2021). DNA Damage-Induced Inflammatory Microenvironment and Adult Stem Cell Response. Front. Cell Dev. Biol. *9*, 729136. 10.3389/FCELL.2021.729136/BIBTEX.

2. Chatzinikolaou, G., Karakasilioti, I., and Garinis, G.A. (2014). DNA damage and innate immunity: Links and trade-offs. Trends Immunol. *35*, 429–435. 10.1016/j.it.2014.06.003.

3. McLaughlin, M., Patin, E.C., Pedersen, M., Wilkins, A., Dillon, M.T., Melcher, A.A., and Harrington, K.J. (2020). Inflammatory microenvironment remodelling by tumour cells after radiotherapy at Nature Research, 10.1038/s41568-020-0246-1 10.1038/s41568-020-0246-1.

4. Reisländer, T., Groelly, F.J., and Tarsounas, M. (2020). DNA Damage and Cancer Immunotherapy: A STING in the Tale. Mol. Cell *80*, 21–28. 10.1016/j.molcel.2020.07.026.

5. Ka, N.L., Lim, G.Y., Hwang, S., Kim, S.S., and Lee, M.O. (2021). IFI16 inhibits DNA repair that potentiates type-I interferon-induced antitumor effects in triple negative breast cancer. Cell Rep. *37*, 110138. 10.1016/j.celrep.2021.110138.

6. Beumer, J., and Clevers, H. (2024). Hallmarks of stemness in mammalian tissues. Cell Stem Cell *31*, 7–24. 10.1016/j.stem.2023.12.006.

7. Yu, Q., Katlinskaya, Y. V., Carbone, C.J., Zhao, B., Katlinski, K. V., Zheng, H., Guha, M., Li, N., Chen, Q., Yang, T., et al. (2015). DNA-Damage-Induced Type I Interferon Promotes Senescence and Inhibits Stem Cell Function. Cell Rep. *11*, 785–797. 10.1016/j.celrep.2015.03.069.

8. Vitale, I., Manic, G., De Maria, R., Kroemer, G., and Galluzzi, L. (2017). DNA Damage in Stem Cells. Mol. Cell *66*, 306–319. 10.1016/j.molcel.2017.04.006.

9. Leibowitz, B.J., Zhao, G., Wei, L., Ruan, H., Epperly, M., Chen, L., Lu, X., Greenberger, J.S., Zhang, L., and Yu, J. (2021). Interferon b drives intestinal regeneration after radiation. Sci. Adv. *7*, 1–13. 10.1126/sciadv.abi5253.

10. Leeman, J.E., Romesser, P.B., Zhou, Y., McBride, S., Riaz, N., Sherman, E., Cohen, M.A., Cahlon, O., and Lee, N. (2017). Proton therapy for head and neck cancer: expanding the therapeutic window. Lancet Oncol. *18*, e254–e265. 10.1016/S1470-2045(17)30179-1.

11. Alan Mitteer, R., Wang, Y., Shah, J., Gordon, S., Fager, M., Butter, P.P., Jun Kim, H., Guardiola-Salmeron, C., Carabe-Fernandez, A., and Fan, Y. (2015). Proton beam radiation induces DNA damage and cell apoptosis in glioma stem cells through reactive oxygen species. Sci. Rep. *5*, 1–12. 10.1038/srep13961.

12. Schniewind, I., Hadiwikarta, W.W., Grajek, J., Poleszczuk, J., Richter, S., Peitzsch, M., Müller, J., Klusa, D., Beyreuther, E., Löck, S., et al. (2022). Cellular plasticity upon proton irradiation determines tumor cell radiosensitivity. Cell Rep. *38*. 10.1016/j.celrep.2022.110422.

13. Sioen, S., Vanhove, O., Vanderstraeten, B., De Wagter, C., Engelbrecht, M., Vandevoorde, C., De Kock, E., Van Goethem, M.J., Vral, A., and Baeyens, A. (2023). Impact of proton therapy on the DNA damage induction and repair in

hematopoietic stem and progenitor cells. Sci. Rep. *13*, 1–8. 10.1038/s41598-023-42362-0.

14. Frame, C.M., Chen, Y., Gagnon, J., Yuan, Y., Ma, T., Dritschilo, A., and Pang, D. (2022). Proton induced DNA double strand breaks at the Bragg peak: Evidence of enhanced LET effect. Front. Oncol. *12*, 1–8. 10.3389/fonc.2022.930393.

15. Maimets, M., Rocchi, C., Bron, R., Pringle, S., Kuipers, J., Giepmans, B.N.G., Vries, R.G.J., Clevers, H., De Haan, G., Van Os, R., et al. (2016). Stem Cell Reports Ar ticle Long-Term In Vitro Expansion of Salivary Gland Stem Cells Driven by Wnt Signals. 10.1016/j.stemcr.2015.11.009.

16. Lühr, A., von Neubeck, C., Krause, M., and Troost, E.G.C. (2018). Relative biological effectiveness in proton beam therapy – Current knowledge and future challenges. Clin. Transl. Radiat. Oncol. *9*, 35. 10.1016/J.CTRO.2018.01.006.

17. Chen, C., and Xu, P. (2023). Cellular functions of cGAS-STING signaling. Trends Cell Biol. *33*, 630–648. 10.1016/j.tcb.2022.11.001.

18. Marchi, S., Guilbaud, E., Tait, S.W.G., Yamazaki, T., and Galluzzi, L. (2023). Mitochondrial control of inflammation. Nat. Rev. Immunol. *23*, 159–173. 10.1038/s41577-022-00760-x.

19. Lei, Y., VanPortfliet, J.J., Chen, Y.F., Bryant, J.D., Li, Y., Fails, D., Torres-Odio, S., Ragan, K.B., Deng, J., Mohan, A., et al. (2023). Cooperative sensing of mitochondrial DNA by ZBP1 and cGAS promotes cardiotoxicity. Cell *186*, 3013-3032.e22. 10.1016/j.cell.2023.05.039.

20. Maekawa, H., Inoue, T., Ouchi, H., Jao, T.M., Inoue, R., Nishi, H., Fujii, R., Ishidate, F., Tanaka, T., Tanaka, Y., et al. (2019). Mitochondrial Damage Causes Inflammation via cGAS-STING Signaling in Acute Kidney Injury. Cell Rep. *29*, 1261-1273.e6. 10.1016/j.celrep.2019.09.050.

21. Victorelli, S., Salmonowicz, H., Chapman, J., Martini, H., Vizioli, M.G., Riley, J.S., Cloix, C., Hall-Younger, E., Machado Espindola-Netto, J., Jurk, D., et al. (2023). Apoptotic stress causes mtDNA release during senescence and drives the SASP. Nature *622*, 627–636. 10.1038/s41586-023-06621-4.

22. Lee, W., Choi, H.I., Kim, M.J., and Park, S.Y. (2008). Depletion of mitochondrial DNA up-regulates the expression of MDR1 gene via an increase in mRNA stability. Exp. Mol. Med. *40*, 109–117. 10.3858/emm.2008.40.1.109.

23. Szczesny, B., Marcatti, M., Ahmad, A., Montalbano, M., Brunyánszki, A., Bibli, S.I., Papapetropoulos, A., and Szabo, C. (2018). Mitochondrial DNA damage and subsequent activation of Z-DNA binding protein 1 links oxidative stress to inflammation in epithelial cells. Sci. Rep. *8*, 1–11. 10.1038/s41598-018-19216-1.

24. Nassour, J., Aguiar, L.G., Correia, A., Schmidt, T.T., Mainz, L., Przetocka, S., Haggblom, C., Tadepalle, N., Williams, A., Shokhirev, M.N., et al. (2023). Telomere-to-mitochondria signalling by ZBP1 mediates replicative crisis. Nature *614*, 767–773. 10.1038/s41586-023-05710-8.

25. Zevini, A., Olagnier, D., and Hiscott, J. (2017). Crosstalk between Cytoplasmic

RIG-I and STING Sensing Pathways. Trends Immunol. *38*, 194–205. 10.1016/j.it.2016.12.004.

26. Thoresen, D.T., Galls, D., Götte, B., Wang, W., and Pyle, A.M. (2023). A rapid RIG-I signaling relay mediates efficient antiviral response. Mol. Cell *83*, 90-104.e4. 10.1016/j.molcel.2022.11.018.

27. Chen, Y.G., and Hur, S. (2022). Cellular origins of dsRNA, their recognition and consequences. Nat. Rev. Mol. Cell Biol. *23*, 286–301. 10.1038/s41580-021-00430-1.

28. Zhao, S., Lu, J., Pan, B., Fan, H., Byrum, S.D., Xu, C., Kim, A., Guo, Y., Kanchi, K.L., Gong, W., et al. (2023). TNRC18 engages H3K9me3 to mediate silencing of endogenous retrotransposons. Nature *623*, 633–642. 10.1038/s41586-023-06688-z.

29. Chiappinelli, K.B., Strissel, P.L., Desrichard, A., Li, H., Henke, C., Akman, B., Hein, A., Rote, N.S., Cope, L.M., Snyder, A., et al. (2015). Inhibiting DNA Methylation Causes an Interferon Response in Cancer via dsRNA Including Endogenous Retroviruses. Cell *162*, 974–986. 10.1016/j.cell.2015.07.011.

30. Elsässer, S.J., Noh, K.M., Diaz, N., Allis, C.D., and Banaszynski, L.A. (2015). Histone H3.3 is required for endogenous retroviral element silencing in embryonic stem cells. Nature *522*, 240–244. 10.1038/nature14345.

31. Dopkins, N., O'Mara, M.M., Lawrence, E., Fei, T., Sandoval-Motta, S., Nixon, D.F., and Bendall, M.L. (2022). A field guide to endogenous retrovirus regulatory networks. Mol. Cell *82*, 3763–3768. 10.1016/j.molcel.2022.09.011.

32. Padeken, J., Methot, S.P., and Gasser, S.M. (2022). Establishment of H3K9-methylated heterochromatin and its functions in tissue differentiation and maintenance. Nat. Rev. Mol. Cell Biol. *23*, 623–640. 10.1038/s41580-022-00483-w.

33. Lazure, F., Farouni, R., Sahinyan, K., Blackburn, D.M., Hernández-Corchado, A., Perron, G., Lu, T., Osakwe, A., Ragoussis, J., Crist, C., et al. (2023). Transcriptional reprogramming of skeletal muscle stem cells by the niche environment. Nat. Commun. *14*. 10.1038/s41467-023-36265-x.

34. Wagers, A.J. (2012). The stem cell niche in regenerative medicine. Cell Stem Cell *10*, 362–369. 10.1016/j.stem.2012.02.018.

35. Hauser, B.R., Aure, M.H., Kelly, M.C., Hoffman, M.P., and Chibly, A.M. (2020). Generation of a Single-Cell RNAseq Atlas of Murine Salivary Gland Development. iScience *23*, 101838. 10.1016/j.isci.2020.101838.

36. Yoon, Y.J., Kim, D., Tak, K.Y., Hwang, S., Kim, J., Sim, N.S., Cho, J.M., Choi, D., Ji, Y., Hur, J.K., et al. (2022). Salivary gland organoid culture maintains distinct glandular properties of murine and human major salivary glands. Nat. Commun. *13*, 1–16. 10.1038/s41467-022-30934-z.

37. Xu, X., Xiong, G., Zhang, M., Xie, J., Chen, S., Li, K., Li, J., Bao, Y., Wang, C., and Chen, D. (2022). Sox9+ cells are required for salivary gland regeneration after radiation damage via the Wnt/β-catenin pathway. J. Genet. Genomics *49*, 230–239. 10.1016/j.jgg.2021.09.008.

38. Formeister, E.J., Sionas, A.L., Lorance, D.K., Barkley, C.L., Lee, G.H., and Magness, S.T. (2009). Distinct SOX9 levels differentially mark stem/progenitor populations and enteroendocrine cells of the small intestine epithelium. Am. J. Physiol. - Gastrointest. Liver Physiol. *296*, 1108–1118. 10.1152/ajpgi.00004.2009.

39. Tanaka, J., Senpuku, H., Ogawa, M., Yasuhara, R., Ohnuma, S., Takamatsu, K., Watanabe, T., Mabuchi, Y., Nakamura, S., Ishida, S., et al. (2022). Human induced pluripotent stem cell-derived salivary gland organoids model SARS-CoV-2 infection and replication. Nat. Cell Biol. *24*, 1595–1605. 10.1038/s41556-022-01007-6.

40. Horton, I., Kelly, C.J., Dziulko, A., Simpson, D.M., and Chuong, E.B. (2023). Mouse B2 SINE elements function as IFN-inducible enhancers. Elife *12*, 1–24. 10.7554/eLife.82617.

41. Steenbakkers, R.J.H.M., van Rijn–Dekker, M.I., Stokman, M.A., Kierkels, R.G.J., van der Schaaf, A., van den Hoek, J.G.M., Bijl, H.P., Kramer, M.C.A., Coppes, R.P., Langendijk, J.A., et al. (2022). Parotid Gland Stem Cell Sparing Radiation Therapy for Patients With Head and Neck Cancer: A Double-Blind Randomized Controlled Trial. Int. J. Radiat. Oncol. Biol. Phys. *112*, 306–316. 10.1016/j.ijrobp.2021.09.023.

42. Van Luijk, P., Pringle, S., Deasy, J.O., Moiseenko, V. V., Faber, H., Hovan, A., Baanstra, M., Van Der Laan, H.P., Kierkels, R.G.J., Van Der Schaaf, A., et al. (2015). Sparing the region of the salivary gland containing stem cells preserves saliva production after radiotherapy for head and neck cancer. Sci. Transl. Med. *7*. 10.1126/scitranslmed.aac4441.

43. Nagle, P.W., Hosper, N.A., Barazzuol, L., Jellema, A.L., Baanstra, M., Van Goethem, M.J., Brandenburg, S., Giesen, U., Langendijk, J.A., Van Luijk, P., et al. (2018). Lack of DNA damage response at low radiation doses in adult stem cells contributes to organ dysfunction. Clin. Cancer Res. *24*, 6583–6593. 10.1158/1078-0432.CCR-18-0533.

44. Hintzsche, H., Hemmann, U., Poth, A., Utesch, D., Lott, J., and Stopper, H. (2017). Fate of micronuclei and micronucleated cells. Mutat. Res. - Rev. Mutat. Res. *771*, 85–98. 10.1016/j.mrrev.2017.02.002.

45. Kwon, M., Leibowitz, M.L., and Lee, J.-H. (2020). Small but mighty: the causes and consequences of micronucleus rupture. Exp. Mol. Med. *52*, 1234567890. 10.1038/s12276-020-00529-z.

46. Cinat, D., Souza, A.L. De, Soto-gamez, A., Jellema-de, A.L., Coppes, R.P., and Barazzuol, L. (2023). Mitophagy induction improves salivary gland stem/progenitor cell function by reducing senescence after irradiation. Radiother. Oncol., 110028. 10.1016/j.radonc.2023.110028.

47. Irazoki, A., Gordaliza-Alaguero, I., Frank, E., Giakoumakis, N.N., Seco, J., Palacín, M., Gumà, A., Sylow, L., Sebastián, D., and Zorzano, A. (2023). Disruption of mitochondrial dynamics triggers muscle inflammation through interorganellar contacts and mitochondrial DNA mislocation. Nat. Commun. *14*. 10.1038/s41467-022-35732-1.

48. Kuriakose, T., and Kanneganti, T.D. (2018). ZBP1: Innate Sensor Regulating Cell Death and Inflammation. Trends Immunol. *39*, 123–134. 10.1016/j.it.2017.11.002.

49. Du, J., Kageyama, S.I., Yamashita, R., Tanaka, K., Okumura, M., Motegi, A., Hojo, H., Nakamura, M., Hirata, H., Sunakawa, H., et al. (2023). Transposable elements potentiate radiotherapy-induced cellular immune reactions via RIG-I-mediated virus-sensing pathways. Commun. Biol. *6*, 1–13. 10.1038/s42003-023-05080-x.

50. Kong, Y., Rose, C.M., Cass, A.A., Williams, A.G., Darwish, M., Lianoglou, S., Haverty, P.M., Tong, A.J., Blanchette, C., Albert, M.L., et al. (2019). Transposable element expression in tumors is associated with immune infiltration and increased antigenicity. Nat. Commun. *10*. 10.1038/s41467-019-13035-2.

51. De Cecco, M., Ito, T., Petrashen, A.P., Elias, A.E., Skvir, N.J., Criscione, S.W., Caligiana, A., Brocculi, G., Adney, E.M., Boeke, J.D., et al. (2019). L1 drives IFN in senescent cells and promotes age-associated inflammation. Nature *566*, 73–78. 10.1038/s41586-018-0784-9.

52. Liu, X., Liu, Z., Wu, Z., Ren, J., Fan, Y., Sun, L., Cao, G., Niu, Y., Zhang, B., Ji, Q., et al. (2023). Resurrection of endogenous retroviruses during aging reinforces senescence. Cell *186*, 287-304.e26. 10.1016/j.cell.2022.12.017.

53. Lawson, H.A., Liang, Y., and Wang, T. (2023). Transposable elements in mammalian chromatin organization. Nat. Rev. Genet. *24*, 712–723. 10.1038/s41576-023-00609-6.

54. Avgustinova, A., Laudanna, C., Pascual-García, M., Rovira, Q., Djurec, M., Castellanos, A., Urdiroz-Urricelqui, U., Marchese, D., Prats, N., Van Keymeulen, A., et al. (2021). Repression of endogenous retroviruses prevents antiviral immune response and is required for mammary gland development. Cell Stem Cell *28*, 1790-1804.e8. 10.1016/j.stem.2021.04.030.

55. Clapes, T., Polyzou, A., Prater, P., Sagar, Morales-Hernández, A., Ferrarini, M.G., Kehrer, N., Lefkopoulos, S., Bergo, V., Hummel, B., et al. (2021). Chemotherapy-induced transposable elements activate MDA5 to enhance haematopoietic regeneration. Nat. Cell Biol. *23*, 704–717. 10.1038/s41556-021-00707-9.

56. Rocchi, C., Cinat, D., Martinez, P.S., Jellema-De Bruin, A.L., Baanstra, M., Brouwer, U., del Angel Zuivre, C., Schepers, H., van Os, R., Barazzuol, L., et al. (2021). The Hippo signaling pathway effector YAP promotes salivary gland regeneration after injury. Sci. Signal. *14*. 10.1126/scisignal.abk0599.

57. Wickham, H. (2016). ggplot2: Elegant Graphics for Data Analysis. Springer-Verlag New York.

58. Robinson, M.D., McCarthy, D.J., and Smyth, G.K. (2009). edgeR: A Bioconductor package for differential expression analysis of digital gene expression data. Bioinformatics *26*, 139–140. 10.1093/bioinformatics/btp616.

59. Wu, T., Hu, E., Xu, S., Chen, M., Guo, P., Dai, Z., Feng, T., Zhou, L., Tang, W., Zhan, L., et al. (2021). clusterProfiler 4.0: A universal enrichment tool for

interpreting omics data. Innovation *2*, 100141. 10.1016/j.xinn.2021.100141.

60. Supek, F., Bošnjak, M., Škunca, N., and Šmuc, T. (2011). Revigo summarizes and visualizes long lists of gene ontology terms. PLoS One *6*. 10.1371/journal.pone.0021800.

61. Liao, Y., Smyth, G.K., and Shi, W. (2019). The R package Rsubread is easier, faster, cheaper and better for alignment and quantification of RNA sequencing reads. Nucleic Acids Res. *47*. 10.1093/nar/gkz114.

62. Hao, Y., Hao, S., Andersen-Nissen, E., Mauck, W.M., Zheng, S., Butler, A., Lee, M.J., Wilk, A.J., Darby, C., Zager, M., et al. (2021). Integrated analysis of multimodal single-cell data. Cell *184*, 3573-3587.e29. 10.1016/j.cell.2021.04.048.

63. He, J., Babarinde, I.A., Sun, L., Xu, S., Chen, R., Shi, J., Wei, Y., Li, Y., Ma, G., Zhuang, Q., et al. (2021). Identifying transposable element expression dynamics and heterogeneity during development at the single-cell level with a processing pipeline scTE. Nat. Commun. *12*, 1–14. 10.1038/s41467-021-21808-x.

64. F. Alexander Wolf1* , Philipp Angerer1 and Fabian J. Theis1, 2* (2018). SCANPY: large-scale single-cell gene expression data analysis. Genome Biol. *19*. https://doi.org/10.1186/s13059-017-1382-0.